Journal of Materials Chemistry A

Accepted Manuscript

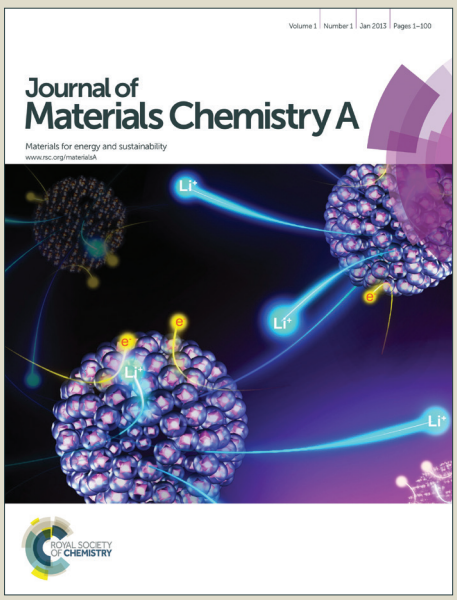

ROYAL SOCIETY OF CHEMISTRY

www.rsc.org/materialsA

Journal Name

ARTICLE

Synergistic enhancement and mechanism study of mechanical and moisture stability of perovskite solar cell introducing polyethylene -imine into $CH_3NH_3PbI_3$/HTM interface

Received 00th January 20xx,
Accepted 00th January 20xx

DOI: 10.1039/x0xx00000x

www.rsc.org/

Jae Hoon Yun,[a,b] Inhwa Lee,[c] Taek-Soo Kim,[c] Min Jae Ko,[a,d] Jin Young Kim,[a] and Hae Jung Son[a,b]*

High performance perovskite solar cells with high stability in moist air are required for their practical applications. We have developed a simple approach to enhancing device stability via the introduction of a polyethyleneimine (PEI) compatibilizer between the perovskite ($CH_3NH_3PbI_3$) and upper hole transporting layers (HTMs). The PEI effectively reduces moisture intrusion into the $CH_3NH_3PbI_3$ layer under a high humidity condition. Moreover, the incorporation of PEI increases the adhesion at the $CH_3NH_3PbI_3$/HTM interface, which makes the protective HTM strongly adhere onto the $CH_3NH_3PbI_3$ layer during degradation and significantly decreases direct exposure of $CH_3NH_3PbI_3$ to moist air. As a result, the solar cell device was found to exhibit remarkably improved moisture stability, maintaining a performance of 85% for 14 days of exposure to 85% relative humidity without any encapsulation. We investigated the effects of the PEI introduction on the perovskite solar cell properties and demonstrated for the first time that the strong adhesion of the $CH_3NH_3PbI_3$/HTM layer results in the perovskite solar cell device that is not only mechanically stable but also exhibits high long-term stability.

Introduction

The performances of photovoltaic devices based on organometallic halide perovskites (e.g., the methylammonium lead halides $CH_3NH_3PbX_3$, where X = halogen) have improved rapidly,[1–9] with power conversion efficiencies (PCEs) now reported in excess of 20%.[10] In contrast to current commercial solar cell technologies, perovskite-based solar cells can be easily fabricated by using cost-effective solution processes such as spray-coating, spin-coating, slot-die coating, and roll-to-roll coating under ambient conditions, which highlights their potential of replacing silicon-based solar cells and revolutionizing the renewable energy market.[11–17] In spite of the progress in efficiency, a number of technical challenges must be overcome if perovskite solar cells are to become suitable for commercial applications. These challenges include finding a replacement for their lead component, large-scale device fabrication, and ensuring long-term device stability.[14,18–24] The low stability of $CH_3NH_3PbX_3$, where X = halogen, remains a major issue; in particular, moisture causes the decomposition of $CH_3NH_3PbX_3$ perovskites in solar cell devices and thereby significantly reduces the device performance.[25–29]

Recently, it has been recognized that HTMs have a key role in enhancing not only solar cell efficiency but also device stability. An HTM layer can have a protective effect on a perovskite layer by shielding it from atmospheric moisture, as well as sealing in the volatile perovskite components and preventing the thermally induced loss of the organic molecules.[30,31] Such protection is known to be strongly dependent on the properties of the HTM such as permeability, hydrophobicity, and molecular density. There have been several reports of HTMs with low moisture permeability. Snaith and co-workers reported that employing P3HT/SWNTs-PMMA as the HTM can improve device resistance to moisture,[25] and that an Al_2O_3 protecting interlayer[19] and a hydrophobic oligothiophene HTM[32] can both protect an underlying perovskite film. Wei *et al.*[33] fabricated a solar cell device containing $CH_3NH_3PbI_3$ and a carbon electrode bilayer, which was found to retain ~90% of its initial performance after storage in a relative humidity (RH) of 30% for 12 days. Strong adhesion between the perovskite and HTM layers is also important because delamination of the HTM from the perovskite layer during device degradation can accelerate perovskite decomposition by directly exposing the perovskite layer to the atmosphere. More importantly, enhanced adhesion can enable the production of flexible solar cell devices with high mechanical stability. Therefore, in this study, we attempted to engineer the interface between the

[a] Photoelectronic Hybrid Research Center, Korea Institute of Science and Technology (KIST), Seoul, Republic of Korea Address here.
[b] Department of Nanomaterials Science and Engineering, University of Science and Technology (UST), Daejeon, Republic of Korea Address here.
[c] Department of Mechanical Engineering, Korea Advanced Institute of Science and Technology (KAIST), Daejeon 305-701, Republic of Korea
[d] KU-KIST Graduate School of Converging Science and Technology Korea University Seoul 136-701, Republic of Korea
E-mail: hjson@kist.re.kr

† Electronic Supplementary Information (ESI) available: Experimental details for solar cell measurements, device fabrication and XRD, XPS, SEM and EDS measurements. See DOI: 10.1039/x0xx00000x

perovskite and HTM layers in order to enhance the adhesion and minimize moisture attacks.

In this study, we searched for an organic polymer with amine groups that can effectively bind metals such as Pb. Such polymer would be a good compatibilizer for the perovskite and the HTM because carbon-based organic polymers usually exhibit effective intermolecular interactions with organic HTMs. Based on this idea, polyethyleneimine (PEI) was chosen and introduced between the perovskite active layer and the HTM layer in the perovskite solar cell. Our observations demonstrate that PEI provides strong adhesion between the $CH_3NH_3PbI_3$ and HTM layers, implying that the device exhibits improved mechanical stability in delamination testing. Moreover, the hydrophilic PEI deposited on the $CH_3NH_3PbI_3$ layer traps H_2O existing inside the device and effectively suppresses its migration into the $CH_3NH_3PbI_3$ layer. As a result, the introduction of the PEI remarkably enhances not only the mechanical stability of the solar cell device by improving the adhesion of $CH_3NH_3PbI_3$ with the HTM but also its moisture stability. This article reports our systematic assessment of the effects of introducing PEI into the perovskite solar cell on its photovoltaic properties and its device stability in 85% RH.

RESULTS AND DISCUSSION

We prepared a meso-structured perovskite solar cell with the configuration FTO/TiO_2 compact layer/mesoporous TiO_2/$CH_3NH_3PbI_3$/HTM/Au by modifying a previously reported method[34,35] and using 2,2′,7,7′-tetrakis(N,N-di-p-methoxyphenylamine)9,9′-spirobifluorene (spiro-OMeTAD) as the hole transporter.The perovskite $CH_3NH_3PbI_3$ was deposited with a two-step sequential deposition method and the resulting perovskite film was coated with a PEI solution dissolved in toluene. The preparation conditions and procedures are described in detail in the Supporting Information. Figure 1 (b) shows a scanning electron microscopy (SEM) image of the surface morphology of the prepared film, which is similar to that of the surface before PEI coating (Figure 1(a)). Most of the surface was composed with small crystallites in the range of 100-200 nm. After coating the perovskite surface has a decreased contact angle (23.3°) with a water drop compared to that before coating (37.7°), which indicates that the hydrophilic PEI covers the whole perovskite surface. Figure 1(c) shows a cross-section SEM image of the FTO/TiO_2 compact layer/mesoporous TiO_2/$CH_3NH_3PbI_3$(with PEI)/HTM before Au evaporation, consisting of ~400 nm $CH_3NH_3PbI_3$ filled in the mesoporous TiO_2 including a perovskite capping layer. The UV-vis absorption spectra shown in Figure 1(d) of the stacked films before and after PEI coating, which contain the characteristic absorption of $CH_3NH_3PbI_3$, are very similar. The X-ray diffraction (XRD) peak pattern of the structure after PEI coating in Figure 1(e) is almost identical to that before coating, and is in accord with a tetragonal perovskite crystal structure, which is the most stable phase at room temperature; in this crystal structure, 6-fold-coordinated Pb^{2+} cations occupy the corners of the unit cell, surrounded by an octahedron of I^- anions, with a $CH_3NH_3^+$ cation filling the space in the middle of the unit cell. Thus the introduction of the PEI coating does not significantly affect the properties of the perovskite layer, although the PEI deposited perovskite surface does become more hydrophilic. The exact thickness of the PEI film could not be determined and however, is thought very thin of several nm.

To determine the properties of the upper part of the perovskite layer, which is the part of the layer directly influenced by the PEI coating, we performed X-ray photoelectron spectroscopy (XPS) on the perovskite layer before and after PEI coating; the XPS spectra are shown in Figure 2. The dashed lines in the spectra mark the core energy levels corresponding to C 1s, Pb 4f, I 3d, and N 1s. In Figures 2(a) and (b), the spectrum of the PEI-coated perovskite contains a C 1s peak that is more pronounced than that in the spectrum of the uncoated perovskite, and it also contains a new N 1s peak due to NH_2 or NH. In Figs. 3(c) and (d), the I 3d and Pb 4f core

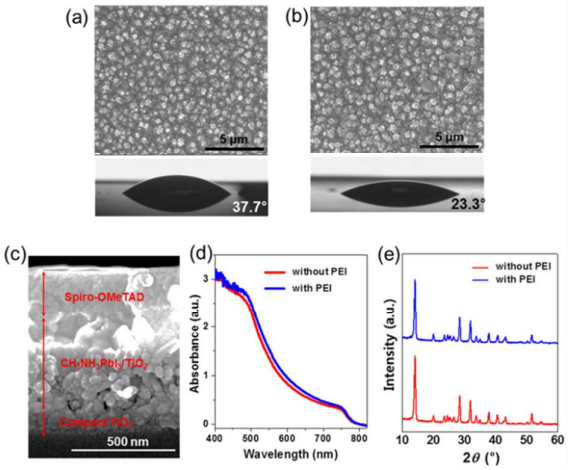

Figure 1. Top-view SEM images of perovskite films and corresponding H_2O drops on the surfaces showing contact angles (a) before and (b) after the PEI coating. (c) A SEM cross-sectional image of the device with PEI before Au evaporation. (d) UV-vis absorption spectra and (e) XRD patterns of the perovskite films.

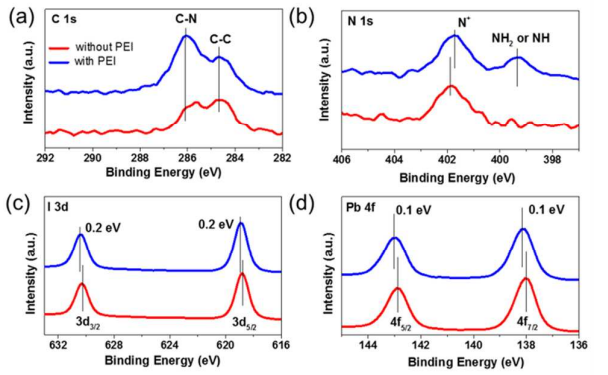

Figure 2. XPS spectra of the perovskite films of (a) C 1s, (b) N 1s, (c) I 3d, and (d) Pb 4f.

levels of the PEI-coated perovskite are shifted simultaneously by 0.2 and 0.1 eV respectively with respect to their initial values in the spectrum of the uncoated perovskite. There are no new characteristic peaks in the spectrum of the coated perovskite. This result suggests that no new chemical bonds have formed between Pb^{2+} and the amine groups of PEI even though Pb^{2+} usually bonds well with amine compounds,[36–39] and that the perovskite structure is well conserved. Instead, electron-rich nitrogen atoms of PEI are likely to interact attractively with the electropositive sites in the perovskite such as I^+, H^+, and Pb^{2+}.

Figure S1(a) shows the J-V curves of the fabricated solar cell devices. The device achieved a power conversion efficiency (PCE) of 13.48%, averaged over forward and backward scans, with a short circuit current (J_{sc}) of 18.30 mA/cm^2, an open circuit voltage (V_{oc}) of 1.0 V, and a fill factor (FF) of 73.64%. The integrated current obtained from the external quantum efficiency (EQE) spectrum (Figure S1(b)) was 18.2 mA/cm^2. This performance is comparable to that of the solar cell device without PEI, which was found to exhibit a PCE of 12.98%, averaged over forward and backward scans, with a J_{sc} of 19.11 mA/cm^2, a V_{oc} of 0.98 V, and a FF of 69.32% (Figure S2). Photoluminescence (PL) and time-resolved photoluminescence (TRPL) decay experiments were performed to study the effect of PEI incorporation on hole injection from the $CH_3NH_3PbI_3$ ($MAPbI_3$) absorbing layer to the spiro-OMeTAD HTM. The $MAPbI_3$ layer was prepared on a cleaned glass substrate by spin-coating and then, PEI and spiro-OMeTAD were coated in sequene on the top of the $CH_3NH_3PbI_3$ layer. For comparison, a $MAPbI_3$/spiro-OMeTAD film without PEI was also prepared using the same condition. The detailed experiment conditions are described in Supporting Information. PL decay times (τ_es) of the prepared films, where τ_e is the time taken for the PL to fall to 1/e of its initial intensity, were measured to compare the PL lifetimes of $MAPbI_3$ of each film as shown in Figure S3 (a). The τ_e of the pristine $MAPbI_3$ was 10.19 ns. For the samples with spiro-OMeTAD, τ_es of $MAPbI_3$ were measured to be 1.44 and 3.23 ns for the films with and without PEI, respectively. This implies the hole transfer from the $CH_3NH_3PbI_3$ layer to the HTM of the film with PEI is a little more efficient compared with the film without PEI. PL measurements showed a consistent result to the TRPL experiment. In Figure S3 (b), the HTM with PEI led to more efficient PL quenching of the $CH_3NH_3PbI_3$ layer than the HTM without PEI. The PEI incorporation is thought to induce a better contact between the $CH_3NH_3PbI_3$ and HTM layers, resulting in more efficient hole extraction from the $CH_3NH_3PbI_3$ layer to the HTM and thus, slightly enhanced solar cell performnces of the PEI-based solar cell device.

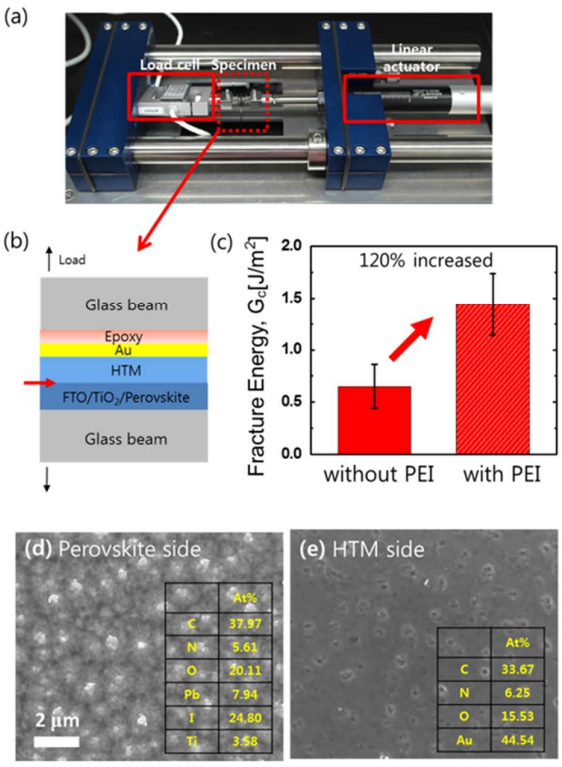

Figure 3. (a) A photograph of the micromechanical test system for DCB test and (b) a schematic of the DCB specimen. (c) Fracture energies measured with and without PEI device specimens. (d, e) SEM images of the fractured surfaces of the device with PEI and the surface atomic compositions (At%) determined from EDS analysis.

To investigate the role of PEI on mechanical stability at the interface between the perovskite and HTM layer, the fracture energies of the samples with and without PEI were measured by double cantilever beam (DCB) testing method.[40-43] The sandwiched structure specimens were fabricated for the DCB test as shown in figure 3(a, b). The fracture energy value of 1.44 ± 0.30 J/m^2 was measured with PEI and it is 120% larger than that of the specimen without PEI, which is 0.65 ± 0.21 J/m^2 (Figure 3(c)). The crack path was identified by using SEM and energy-dispersive x-ray spectroscopy (EDS) analysis. Figure 3(d, e) shows SEM images of the fractured surfaces of the device with PEI. The SEM image of the upper surface (Figure 3(e)) shows holes of ~300 nm diameters which match exactly with the bottom surface morphology (Figure 3(d)). In Figure 3(d), the image resembles the surface of the perovskite but HTM layer is slightly covered on it. EDS results show that Pb and I, which are key elements for perovskite, were only detected for the bottom surface (Figure 3(d)). It is inferred that the sharp and pointed region on the top of perovskite were pulled out from the HTM. However, the HTM layer which has deeply penetrated into perovskite was not detached during the delamination process. The device without PEI in Figure S4 shows the same crack path to that of PEI based device. From these results, it is derived that the $CH_3NH_3PbI_3$/HTM interface is the mechanically weakest part among the layers in the meso-structured perovskite solar cell device.

In order to explore the enhancement mechanism of PEI on the fracture energy, the detached surfaces were characterized after DCB test. Surprisingly, even though the fracture energy was increased by 120%, it was difficult to find any mechanical mechanisms such as crack bridging and mechanical

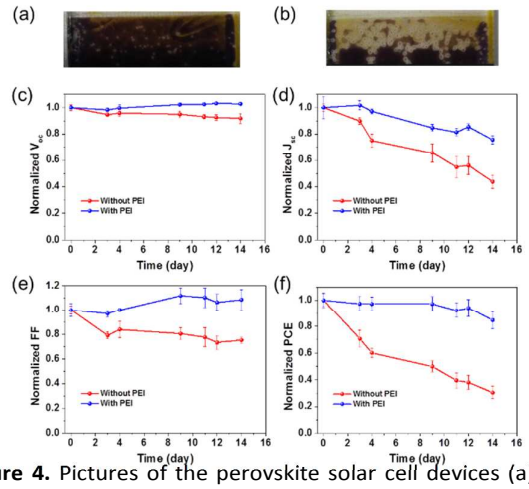

Figure 4. Pictures of the perovskite solar cell devices (a) with and (b) without PEI under 85% humidity at room temperature after 14 days and (c-f) the corresponding normalized photovoltaic properties (average values of 20 devices fabricated under identical conditions) monitored as a function of time.

interlocking depending on the PEI's existence from the above SEM and EDS results. Also, the crack paths for both specimens with and without PEI were identical, which suggests that the fracture energy increase is due to the chemical bonding formed at the interface rather than mechanical interlocking. The fracture energy value of 0.65 ± 0.21 J/m^2 is similar to the van der Waals adhesion energy of 0.72 ± 0.07 J/m^2 for the interaction between the graphene and the metal. [42] Therefore, it can be presumed that the weak fracture energy based on van der Waals force has increased with chemical interaction formed by PEI. PEI is expected to interact favourably with both $CH_3NH_3PbI_3$ and spiro-OMeTAD and thus to enable strong adhesion between the HTM and perovskite layers. The intermolecular interactions between nitrogen of amine compounds and Pb of $CH_3NH_3PbI_3$ are well known. We found that a 1H NMR peak corresponding to N-H of PEI was shifted up-field from 2.0 ppm to 1.9 ppm when excess amounts of spiro-OMeTAD were added into the PEI solution in $CDCl_3$, which indicates that there are intermolecular interactions between PEI and spiro-OMeTAD such as N-H_{PEI}···$O_{spiro\text{-}OMeTAD}$. We also studied the surface energy of the perovskite before and after PEI coating by performing contact angle measurements. Contact angles were averaged from measurements of 5 solution drops. A contact angle of the perovskite film with PEI (4.48°) to chlorobenzene was lower than that of the film without PEI (5.16°). The contact angle decrement was larger with a drop of a spiro-OMeTAD solution in chlorobenzene used for device fabrication, from 7.42° before PEI coating to 5.41° after the coating. These results reveal that PEI makes the perovskite film to have increased wettability to the spiro-OMeTAD precursor solution, which enables the formation of better contact between the perovskite and HTM layers with high surface coverage. The improved contact would contribute to the adhesion enhancement at the interface.

The long-term stability of the unencapsulated perovskite solar cell device was studied by monitoring the evolution of the solar cell parameters during exposure to 85% RH at room temperature for 14 days; the results are presented in Figure 4. The stability of the PEI-coated solar cell is significantly better than that of the device prepared with the conventional method. As shown in Figures 4(a) and (b), the coated and uncoated solar cell devices have very different appearances; the device without PEI became light yellow with some brown areas whereas the PEI-coated device was found to maintain its original dark brown color. In Figures 4(c) to (f), the decay of each solar cell parameter averaged over 20 solar cell devices is shown as a function of time. After 14 days at 85% RH, the PEI-coated device retained its initial efficiency up to 85%, whereas there was a significant efficiency reduction in the cell prepared

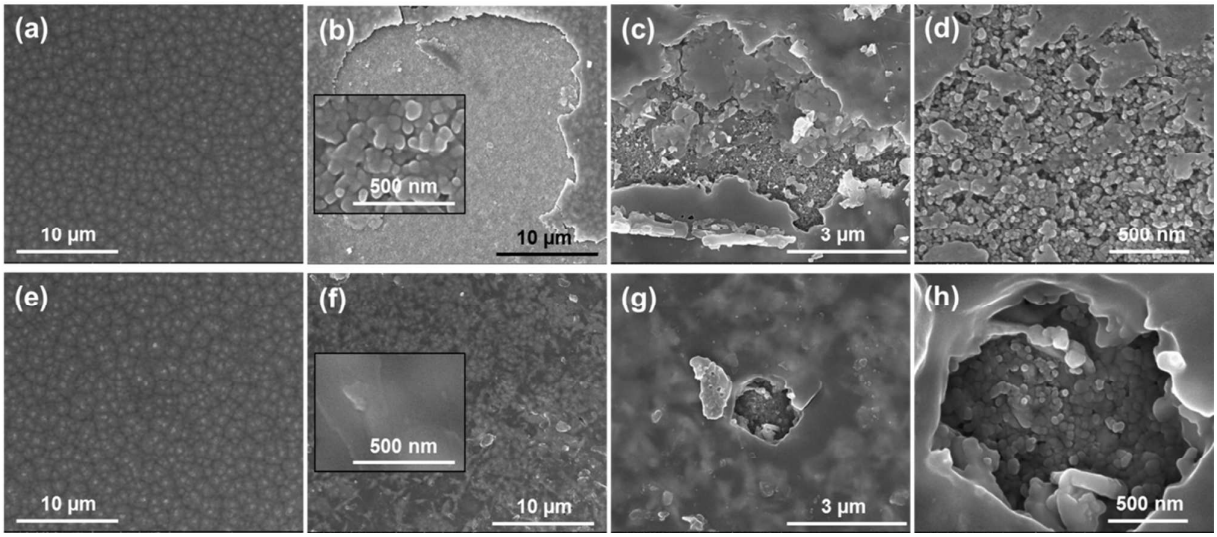

Figure 5. Top-view SEM images of the Au-uncovered areas in the devices without PEI (a-d) and with PEI (e-h). (a, e) Images before degradation. (b-d, f-h) Images after degradation.

with the conventional method, which only retained 35% of its performance before decomposition. This reduction is mostly due to decreases in J_{sc} and FF, although a small V_{oc} reduction (5% reduction) was also observed; the J_{sc} and FF values of the device are reduced to approximately 45% and 75%, respectively of the initial values. In contrast, the device with PEI was found to undergo a relatively small decrease in J_{sc} (a 20% reduction) and FF was almost completely conserved.

We compared the film morphologies of the degraded solar cell devices by using SEM and atomic force microscopy (AFM). The images in Figures 5(b) and (f) of the PEI-based device show that the surface is relatively well conserved without significant decomposition, whereas significant film degradation is evident in the case of the device without PEI; in the decomposed region, the HTM or $CH_3NH_3PbI_3$/HTM layers are fragmented and nanoscale particles thought to be TiO_2 are directly exposed to the surface, as shown in Figures 5(c) and (d). This damage is correlated with the high surface roughness of the degraded film in the AFM image (Figures S5(a) and (b)); the surface root-mean-square (RMS) roughness is increased from an initial 11.5 nm to 66.4 nm by degradation. In contrast, after 14 days, there is only a minor change in the RMS value of most of the surface area of the PEI-based device, from 11.2 nm to 12.3 nm as shown in Figures S5(c) and (d). One interesting point is that the decomposition behaviors of the devices are also very different: in Figures 5(c) and (d), it can be seen that film degradation of the uncoated device occurred *via* the fragmentation of its upper layers into small nanoscale pieces, whereas few large pinholes with a diameter of 1–2 μm are evident for the PEI-coated device and the delaminated part maintained its shape relatively well without further erosion.

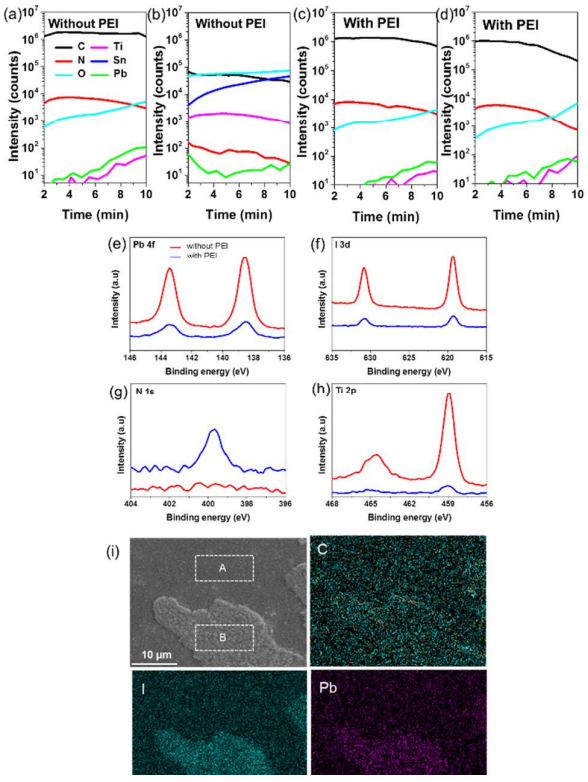

Figure 6. Dynamic-SIMS profiles of the perovskite solar cell devices before (a, c) and after (b, d) degradation. XPS spectra of the perovskite films of (e) Pb 4f, (f) I 3d, (g) N 1s, and (h) Ti 2p after degradation

Secondary ion mass spectrometry (SIMS) measurements were performed on the decomposed part of the PEI uncoated device. Figure 6 displays the dynamic-SIMS depth profiling for initial 10 minutes, which shows the composition of the degraded device in the depth range 150~200 nm from the surface. Before degradation, the level of Pb increases with depth from zero on the surface (Figure 6(a)), whereas the profile of the degraded device indicates that Pb ions are present in similar intensities from the surface to the whole depth (Figure 6(b)). Figure S6 shows that the level of detected S ions is remarkably reduced after decomposition, which indicates that much of the HTM has peeled off from the surface. Note that the signals due to Ti and O elements in the mass spectrum of the degraded device are much more intense than before degradation, which is consistent with the SEM measurements in Figure 5(b); many particles thought to be TiO_2 are exposed due to the exfoliation of the upper layer. We performed XPS on the degraded devices and the results are shown in Figures 6(e) to (h); in the spectrum of the perovskite device without PEI, the Pb 4f and I 3d peaks are much more pronounced than the corresponding peaks of the device with PEI. Notably, for the device without PEI, there is no N 1s peak after decomposition but there is an intense peak corresponding to Ti. Figure 6(i) shows a SEM image and the corresponding energy-dispersive X-ray spectroscopy (EDS) mapping results for the decomposed area in the PEI uncoated device, which indicate the presence of two different types of decomposition: in area B, elemental Pb and I are delocalized homogeneously whereas there are no significant signals for either of them in area A. The atomic ratio of Pb and I in area B is Pb:I=1:2.5, which indicates that most of the perovskite has decomposed to lead iodide compounds such as PbI_2. For both areas A and B, there is a very small signal due to elemental C. Thus, according to the SIMS and XPS data, most of the HTM peels off after decomposition and the perovskite is finally converted to PbI_2. In some areas, TiO_2 particles might be directly exposed to the atmosphere after the decomposed perovskite has peeled off from the device. It has been reported that $CH_3NH_3PbI_3$ can decompose into volatile compounds such as CH_3NH_2 and HI after reaction with H_2O.[18,44] Such gaseous chemicals will cause voids in the perovskite layer, followed by cracking and delamination of the upper layer. After evaporation of such volatile compounds, lead iodide compounds are expected to comprise the majority of the decomposed perovskite layer. In contrast, there are no notable changes in the SIMS intensities of the device with PEI before and after moisture exposure (Figures 6(c) and (d)). The device structure appears relatively well conserved. Thus the

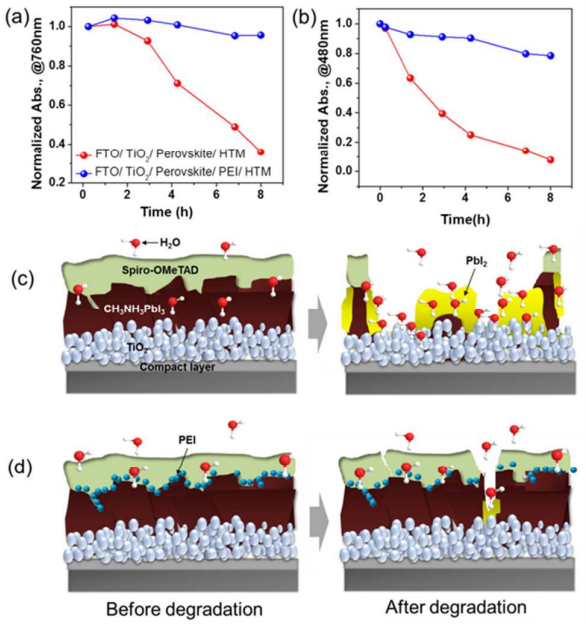

Figure 7. Normalized absorbance at (a) 760 nm and (b) 480 nm as a function of time for FTO/TiO_2/$CH_3NH_3PbI_3$/HTM films exposed to 85% humidity. Cartoon depiction of the structural and morphological difference between the solar cell devices (c) without PEI and (d) with PEI upon exposure to 85% humidity for 14 days.

enhanced adhesion between the perovskite and HTM layers after PEI introduction might effectively reduce delamination of the HTM and thus the degradation of the HTM and perovskite layers.

Figure S7 shows the absorption at 760 nm and 480 nm of $CH_3NH_3PbI_3$/TiO_2/FTO films stored at 85% RH in the dark for 8 h. Over this relatively short time period, the absorption at both 480 nm and 760 nm steadily eroded and the original dark brown of $CH_3NH_3PbI_3$ changed to light yellow. In comparison, there were much smaller decreases in the absorption of the PEI/$CH_3NH_3PbI_3$/TiO_2/FTO film over this period; the absorption peak corresponding to the bandgap at 760 nm is relatively well conserved and the high-energy absorption at 480 nm decreases much more slowly upon exposure to moisture. PEI is more hydrophilic than perovskite, so it is expected that the PEI layer will protect the perovskite layer by keeping H_2O not to permeate into the perovskite layer, and this will slow down the degradation of the perovskite layer. Similar observations have also been reported by Kelly *et al.*: the introduction of a hydrophilic material onto the perovskite layer delays H_2O migration into the perovskite layer by trapping it, and can thus be used to improve the moisture stability of perovskite solar cell devices.[45] Interestingly, when the HTM spiro-OMeTAD was coated on the PEI/perovskite/TiO_2/FTO film, the moisture stability was more improved compared with the film before the HTM coating despite the perovskite/TiO_2/FTO films exhibited similarly low moisture stability regardless the HTM was covered or not (Figure 7(a) and (b)). Once perovskite degradation starts, the perovskite layer will be quickly exposed to the surface and moist air because spiro-OMeTAD is easily broken apart after cracks form in the film.[25,45] Spiro-OMeTAD on the $CH_3NH_3PbI_3$/PEI film can adhere conformally to the underlying perovskite layer, so it can act effectively as a moisture barrier without being delaminated. Figure 7 shows a schematic illustration of the origins of the improved moisture stability of the PEI-treated device: at first, the trapping of moisture by the PEI layer; next, even after some perovskite has decomposed, the protective HTM conformally adheres to the perovskite layer due to the PEI and thus, suppresses further degradation of the perovskite. We demonstrated for the first time that $CH_3NH_3PbI_3$/HTM has low fracture energy, and therefore improving adhesion property at the interface is crucial for the enhancement of mechanical and moisture stability of the solar cell device. The improved stability of the perovskite layer is thought to directly affect the photocurrent properties of the solar cell; the cell device with PEI retains more stable J_{sc} values during degradation, which is probably because the deterioration of absorption and transport properties is much reduced. FF is relatively constant without any significant decrement. These features are mostly due to the well-conserved HTM layer, which minimizes charge recombination by blocking electron transfer and direct contact between the perovskite layer and the electrode.

Conclusions

In conclusion, we have demonstrated the simultaneous improvement of the mechanical and moisture stabilities of perovskite solar cells *via* the highly reliable and simple introduction of a PEI compatibilizer onto the perovskite active layer. The incorporation of PEI increases the adhesion at the perovskite/HTM interface, which improves the moisture stability by tightly binding the protective HTM to the perovskite layer. It is found that PEI effectively retards moisture intrusion into the perovskite layer by retaining it. As a result, the resulting solar cell device was found to exhibit remarkably improved resilience against moisture attack, maintaining 85% of its initial performance for 14 days at 85% RH without any encapsulation. There have been few reports of perovskite solar cells that maintain their performances well at a high relative humidity of 85% for such a long period. This study systematically investigated the effects of PEI post-modification of $CH_3NH_3PbI_3$ on perovskite solar cells, and has opened up a new pathway toward achieving high performance flexible perovskite solar cells with high mechanical stability and long-term moisture stability.

Acknowledgements

This work was supported by the Global Frontier R&D Program on Center for Multiscale Energy System and Basic Science Research Program (2015R1A1A1A05001115) funded by the National Research Foundation under the Ministry of Science, Korea Institute of Science and Technology (KIST) for Project

No. 2E25392, and the New and Renewable Energy Program of the Korea Institute of Energy Technology Evaluation and Planning (KETEP) grant funded by the Korea Government Ministry of Trade, Industry & Energy (MTIE) (20133030000130, 20113030010030).

Notes and references

1 M. M. Lee, J. Teuscher, T. Miyasaka, T. N. Murakami and H. J. Snaith, *Science*, 2012, **338**, 643–647.
2 A. Abrusci, S. D. Stranks, P. Docampo, H.-L. Yip, A. K. Y. Jen and H. J. Snaith, *Nano Lett.*, 2013, **13**, 3124–3128.
3 E. J. W. Crossland, N. Noel, V. Sivaram, T. Leijtens, J. A. Alexander-Webber and H. J. Snaith, *Nature*, 2013, ***495***, 215–219.
4 E. Edri, S. Kirmayer, D. Cahen and G. Hodes, *J. Phys. Chem. Lett.*, 2013, **4**, 897–902.
5 J. H. Heo, S. H. Im, J. H. Noh, T. N. Mandal, C.-S. Lim, J. A. Chang, Y. H. Lee, H.-j. Kim, A. Sarkar, M. K. Nazeeruddin, M. Grätzel and S. I. Seok, *Nat. Photonics*, 2013, **7**, 486–491.
6 M. Liu, M. B. Johnston and H. J. Snaith, *Nature*, 2013, **501**, 395–398.
7 N. J. Jeon, H. G. Lee, Y. C. Kim, J. Seo, J. H. Noh, J. Lee and S. I. Seok, *J. Am. Chem. Soc.*, 2014, **136**, 7837–7840.
8 H. Zhou, Q. Chen, G. Li, S. Luo, T.-b. Song, H.-S. Duan, Z. Hong, J. You, Y. Liu and Y. Yang, *Science*, 2014, **345**, 542–546.
9 K. Wojciechowski, M. Saliba, T. Leijtens, A. Abate and H. J. Snaith, *Energy Environ. Sci.*, 2014, **7**, 1142–1147.
10 W. S. Yang, J. H. Noh, N. J. Jeon, Y. C. Kim, S. Ryu, J. Seo and S. I. Seok, *Science*, 2015, **348**, 1234–1237.
11 H. J. Snaith, *J. Phys. Chem. Lett.*, 2013, **4**, 3623–3630.
12 A. T. Barrows, A. J. Pearson, C. K. Kwak, A. D. F. Dunbar, A. R. Buckley and D. G. Lidzey, *Energy. Environ. Sci.*, 2014, **7**, 2944–2950.
13 M. H. Kumar, N. Yantara, S. Dharani, M. Graetzel, S. Mhaisalkar, P. P. Boix and N. Mathews, *Chem. Commun.*, 2013, **49**, 11089–11091.
14 K. Hwang, Y.-S. Jung, Y.-J. Heo, F. H. Scholes, S. E. Watkins, J. Subbiah, D. J. Jones, D.-Y. Kim and D. Vak, *Adv. Mater.*, 2015, **27**, 1241–1247.
15 L. Etgar, P. Gao, Z. Xue, Q. Peng, A. K. Chandiran, B. Liu, M. K. Nazeeruddin and M. Grätzel, *J. Am. Chem. Soc.*, 2012, **134**, 17396–17399.
16 F. Zabihi and M. Eslamian, *J. Coat. Technol. Res.*, 2015, **12**, 489–503.
17 D. Vak, K. Hwang, A. Faulks, Y. S. Jung, N. Clark, D. Y. Kim, G. J. Wilson and S. E. Watkins, *Adv. Energy Mater.*, 2015, **5**, 1401539.
18 N. K. Noel, S. D. Stranks, A. Abate, C. Wehrenfennig, S. Guarnera, A.-A. Haghighirad, A. Sadhanala, G. E. Eperon, S. K. Pathak, M. B. Johnston, A. Petrozza, L. M. Herz and H. J. Snaith, *Energy Environ. Sci.*, 2014, **7**, 3061–3068.
19 G. Niu, W. Li, F. Meng, L. Wang, H. Dong and Y. Qiu, *J. Mater. Chem. A*, 2014, **2**, 705–710.
20 G. Hodes and D. Cahen, *Nat. Photonics*, 2014, **8**, 87–88.
21 O. Malinkiewicz, A. Yella, Y. H. Lee, G. M. Espallargas, M. Graetzel, M. K. Nazeeruddin and H. J. Bolink, *Nat. Photonics*, 2014, **8**, 128–132.
22 F. Hao, C. C. Stoumpos, D. H. Cao, R. P. H. Chang and M. G. Kanatzidis, *Nat. Photonics*, 2014, **8**, 489–494.
23 M. Gratzel, *Nat. Mater.*, 2014, **13**, 838–842.
24 N. Espinosa, L. Serrano-Luján, A. Urbina and F. C. Krebs, *Sol. Energy Mater. Sol. Cells*, 2015, **137**, 303–310.
25 S. N. Habisreutinger, T. Leijtens, G. E. Eperon, S. D. Stranks, R. J. Nicholas and H. J. Snaith, *Nano Lett.*, 2014, **14**, 5561–5568.
26 J. A. Christians, P. A. Miranda Herrera and P. V. Kamat, *J. Am. Chem. Soc.*, 2015, **137**, 1530–1538.
27 Y. Han, S. Meyer, Y. Dkhissi, K. Weber, J. M. Pringle, U. Bach, L. Spiccia and Y.-B. Cheng, *J. Mater. Chem. A*, 2015, **3**, 8139–8147.
28 Q. Jiang, D. Rebollar, J. Gong, E. L. Piacentino, C. Zheng and T. Xu, *Angew. Chem., Int. Ed.*, 2015, **54**, 7617–7620.
29 G. Niu, X. Guo and L. Wang, *J. Mater. Chem. A*, 2015, **3**, 8970–8980.
30 J. Liu, Y. Wu, C. Qin, X. Yang, T. Yasuda, A. Islam, K. Zhang, W. Peng, W. Chen and L. Han, *Energy Environ. Sci.*, 2014, **7**, 2963–2967.
31 L. K. Ono, S. R. Raga, M. Remeika, A. J. Winchester, A. Gabe and Y. Qi, *J. Mater. Chem. A*, 2015, **3**, 15451–15456.
32 L. Zheng, Y.-H. Chung, Y. Ma, L. Zhang, L. Xiao, Z. Chen, S. Wang, B. Qu and Q. Gong, *Chem. Commun.*, 2014, **50**, 11196–11199.
33 Z. Wei, H. Chen, K. Yan and S. Yang, *Angew. Chem., Int. Ed.*, 2014, **53**, 13239–13243.
34 J. Burschka, N. Pellet, S.-J. Moon, R. Humphry-Baker, P. Gao, M. K. Nazeeruddin and M. Grätzel, *Nature*, 2013, **499**, 316–319.
35 H.-S. Ko, J.-W. Lee and N.-G. Park, *J. Mater. Chem. A*, 2015, **3**, 8808–8815.
36 J. Harrowfield, H. Miyamae, B. Skelton, A. Soudi and A. White, *Aust. J. Chem.*, 1996, **49**, 1121–1125.
37 S.-R. Fan and L.-G. Zhu, *Inorg. Chem.*, 2006, **45**, 7935–7942.
38 N. K. Noel, A. Abate, S. D. Stranks, E. S. Parrott, V. M. Burlakov, A. Goriely and H. J. Snaith, *ACS Nano*, 2014, **8**, 9815–9821.
39 I. Wharf, T. Gramstad, R. Makhija and M. Onyszchuk, *Can. J. Chem.*, 1976, **54**, 3430–3438.
40 I. Lee, S. Kim, J. Yun, I. Park and T.-S. Kim, *Nanotechnology*, 2012, **23**, 485704.
41 S. Kim, B.-H. Jeong, B. K. Hong and T.-S. Kim, *J. Power Sources*, 2014, **270**, 342–348.
42 T. Yoon, W. C. Shin, T. Y. Kim, J. H. Mun, T.-S. Kim and B. J. Cho, *Nano Lett.*, 2012, **12**, 1448–1452.
43 J. Seo, W. S. Chang and T.-S. Kim, *Thin Solid Films*, 2015, **584**, 170–175.
44 J. M. Frost, K. T. Butler, F. Brivio, C. H. Hendon, M. van Schilfgaarde and A. Walsh, *Nano Lett.*, 2014, **14**, 2584–2590.
45 J. Yang, B. D. Siempelkamp, D. Liu and T. L. Kelly, *ACS Nano*, 2015, **9**, 1955–1963.

Figure 7. Normalized absorbance at (a) 760 nm and (b) 480 nm as a function of time for FTO/TiO_2/$CH_3NH_3PbI_3$/HTM films exposed to 85% humidity. Cartoon depiction of the structural and morphological difference between the solar cell devices (c) without PEI and (d) with PEI upon exposure to 85% humidity for 14 days.

TOC

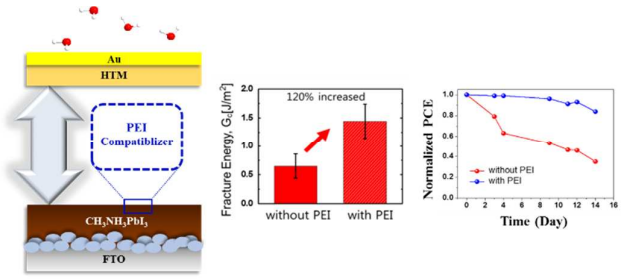

Introduction of polyethyleneimine(PEI) onto the perovskite layer makes HTM strongly adhere to the perovskite layer, which simultaneously enhancing moisture stability.